ELSEVIER

Journal of Photochemistry and Photobiology A: Chemistry 97 (1996) 99–107

Journal of PHOTOCHEMISTRY AND PHOTOBIOLOGY A:CHEMISTRY

Nanoparticles of $SrTiO_3$ prepared by gel to crystallite conversion and their photocatalytic activity in the mineralization of phenol

S. Ahuja [a], T.R.N. Kutty [b,*]

[a] *Department of Organic Chemistry, Indian Institute of Science, Bangalore-560 012, India*

[b] *Materials Research Centre, Indian Institute of Science, Bangalore-560 012, India*

Received 8 November 1995; accepted 20 January 1996

Abstract

Nanometre-sized powders of $SrTiO_3$ were prepared at 70–100 °C by the wet-chemical method of gel to crystallite (G–C) conversion. The crystallite sizes obtained were in the range 5–13 nm, as estimated by transmission electron microscopy (TEM) studies. The photocatalytic activities of these powders in the mineralization of phenol were evaluated in comparison with Degussa P25 (TiO_2). The maximum photocatalytic activity was observed for powders annealed in the range 1100–1300 °C. The optical spectra of the particle suspensions in water showed broadened absorption around the band gap region, together with the appearance of an absorption maximum in the UV region. The effect of inorganic oxidizing species as electron scavengers on the rate of the photocatalytic degradation of phenol was studied. The influence of bulk and surface defects, which participate in the charge transfer process during photocatalysis, was investigated systematically.

Keywords: Photocatalysis; $SrTiO_3$; Degradation; Phenols; Perovskite titanates

1. Introduction

Photoassisted heterogeneous catalysis is the most widely used technique for the mineralization of organic pollutants in water. Ultrafine powders of semiconductor oxides have often been used as photocatalysts, e.g. TiO_2 [1–6], ZnO [7], TiO_2–SiO_2 [8,9] and, to a lesser extent, perovskite titanates such as $SrTiO_3$ [10–12]. The preparative route of the perovskite titanates, and hence the pre-history of the fine powdered particles, plays an important role in determining their photocatalytic activity. In practice, it is difficult to prepare ultrafine powders of mixed oxides because of the high temperature involved in their formation through solid–solid reactions.

A number of methods have been reported for the preparation of $SrTiO_3$ powders at lower temperatures by chemical routes, e.g. hydrothermal synthesis [13,14], chemical coprecipitation [15], precursor method [16] and sol–gel processing [17,18]. Each method has its merits as well as its disadvantages. The wet- chemical synthesis of ultrafine $SrTiO_3$ powders continues to be a subject of intense research activity [19] as the product exhibits many favourable powder characteristics relative to those derived from conventional ceramic routes. The main features are the increased homogeneity and high surface area leading to improved reactivity. Since the wet-chemical synthesis of mixed oxides provides powders with the desired physicochemical properties, innovative methods have been developed and standardized by many groups [19,20].

In this paper, we report the wet-chemical synthesis of nanometre-sized powders of $SrTiO_3$ and metal-doped $SrTiO_3$ by the gel to crystallite (G–C) conversion. The general reaction involved in this technique is the breakdown of the gel network due to the change in ionic pressure brought about by the chemical influx of aliovalent ions [21]. These powders were used as catalysts in the photodegradation of phenol in water.

2. Experimental procedures

Gels of hydrated titania ($TiO_2.xH_2O$ ($80 < x < 130$)) were prepared by the addition of ammonium hydroxide at approximately 40 °C to a solution of titanium oxychloride up to pH 8. The gels were washed free of chloride and ammonium ions. No special care was taken to control the particle size of the gel. The gel was suspended in 0.5 M $Sr(OH)_2$ solution in a flask fitted with a water-cooled reflux condenser. Air in the vessel was displaced by nitrogen. Fresh entry of atmospheric CO_2 was prevented by the use of an alkali guard-tube. The Ti/Sr mole ratio was varied from 0.95 to 1.05. The reaction was carried out at 70–100 °C for 1–4 h with constant

* Corresponding author.

PII 1010-6030(96)04324-9

stirring. The solid phase remaining in the reaction vessel was filtered, washed free of $Sr(OH)_2$ and air dried. The recovered solids were oven dried. They were further annealed at the desired temperature between 110 and 1500 °C. Unlike the titania gel, the solid phases recovered from the G–C conversion were crystalline with X-ray patterns corresponding to a cubic perovskite phase, namely $SrTiO_3$.

$SrTiO_3$ powders doped with transition metal ions (e.g. Mn) were prepared according to the above procedure; the metal salt (more than 0.002 mol.%) was added at the stage of TiO_2 gel preparation.

Phase identification of the powders was carried out by X-ray powder diffraction using a SCINTAG XDS-2000 X-ray diffractometer with a Cu Kα source. The particle size and shape were evaluated by transmission electron microscopy (TEM) using a JEOL 200 CX instrument. The size of the particles was determined by the intercept method from the micrographs. Electron paramagnetic resonance (EPR) spectra of $SrTiO_3$ powders were recorded on a Varian E-109 X-band spectrometer at 9 GHz, with a TE011 cavity, in the range 78–300 K. The absorption spectra were recorded on a Shimadzu UV-2100 UV–visible spectrophotometer. Micromolar suspensions of the particles were prepared by dispersing the powder in water and stirring in an ultrasonic tank for 10 min. Surface area measurements were carried out on a Micromeritics 2200A rapid surface area analyser. Thermal analysis of $SrTiO_3$ powders was carried out in a Polymer Laboratory STA 1500 simultaneous thermogravimetry-differential thermal analysis (TG-DTA) instrument.

Photodegradation experiments were carried out in a silica-glass reactor using a medium pressure mercury vapour lamp source; details of the system have been given elsewhere [22]. Phenol was chosen as a model pollutant, whose initial concentration was 2 mM. The electron scavengers used were H_2O_2 or $NaClO_3$ whose concentration was varied from 20 to 250 mM. The catalyst loading was 0.1 wt.% in all the experiments, and unless otherwise stated all experiments were carried out at pH 6.5. Samples for analysis were withdrawn at the desired intervals of time during irradiation and centrifuged. The concentration of phenol in the supernatant clear solution was determined colorimetrically using the standard method, with 4-amino antipyrine as the reagent [23], on a Hitachi 330 UV–visible spectrophotometer. Calibration was carried out with phenol solutions of known concentrations. CO_2 evolved at low concentrations was measured by sweeping with argon into a Shimadzu gas chromatograph fitted with a Porapak column. At higher concentrations, CO_2 was swept into $Ba(OH)_2$ solution and the precipitated $BaCO_3$ was estimated.

3. Results and discussion

3.1. Characterization of the catalyst

During the initial stages of the G–C conversion reaction, a considerable decrease in gel volume was noted, as a result of the disintegration of the coarse gel caused by the influx of Sr^{2+} ions. As the reaction progressed, the gel lost its appearance and was converted into a flowing powdery mass. The formation of $SrTiO_3$ was complete within 1 h at 100 °C, whereas the reaction time had to be extended to 4 h at 70 °C.

The wet-chemical method of G–C conversion is a simple procedure for the preparation of $MTiO_3$ titanates ($M \equiv$ alkaline earth metal). The method differs from the sol–gel process in that no high temperature calcination is necessary for the formation of crystalline mixed oxides. The mechanism of formation of $MTiO_3$ from coarse titania gel and $M(OH)_2$ has been reported previously [21]. The general feature of G–C conversion involves the instability of $TiO_2.xH_2O$ gel brought about by the change in ionic pressure as a result of the migration of M^{2+} ions through the solvent cavities within the gel framework. The rapid influx of aliovalent M^{2+} ions into the gel cavities containing entrapped solvent can upset the charge balance, and the interactive stability between the gel network and the solvent breaks down. Thus the pH change within the titania gel leads to deolation of the bridging groups, such as Ti–OH–Ti and Ti–O–Ti, followed by oxolation, resulting in the corner-sharing TiO_6 octahedra which are charge compensated by the divalent cation. This results in the collapse of the gel, giving way to fine particles of crystallites under the wet- chemical condition, which is associated with a large decrease in the gel volume, in contrast with the starting stage. The solid recovered from the reaction medium is crystalline as observed by X-ray diffraction (XRD).

The XRD patterns show the formation of single-phase powders with the cubic perovskite structure (Fig. 1(a)) from the G–C conversion reactions. No X-ray reflections arising from rutile (TiO_2) are observed after annealing the powders at high temperatures, indicating the absence of unreacted TiO_2. Heat treatment of the powder is accompanied by a marginal decrease in the cell parameter, as well as a gradual decrease in the half-bandwidth of the X-ray reflections and a gain in the peak heights. The unit cell parameter decreases from $a_0 = 3.936$ Å for the oven-dried sample to $a_0 = 3.910$ Å for the samples annealed above 1100 °C (Fig. 1(b)).

TEM studies (Fig. 2) indicate that the powder particles are nanometre sized, approximately spherical in shape and in the size range 5–13 nm. The corresponding electron diffraction pattern is spotty, indicative of the monocrystallite nature of the particles.

The results of the surface area measurements are shown in Table 1. The surface area of the oven-dried sample (110 °C) is the highest, i.e. 46.7 $m^2 g^{-1}$ (SA-1). As the sample is heat treated, the surface area decreases and reaches a value of 18.6 $m^2 g^{-1}$ (SA-6) for the sample annealed at 1450 °C. A minor weight change of 0.6% is noted in the region 200–1000 °C on the thermogravimetric analysis (TGA) curve when the $SrTiO_3$ powders are subjected to thermal analysis. However, no exothermic peak corresponding to the recrystallization of the amorphous fraction is observed in the DTA curve. The evolved gas analysis shows only water vapour as the product

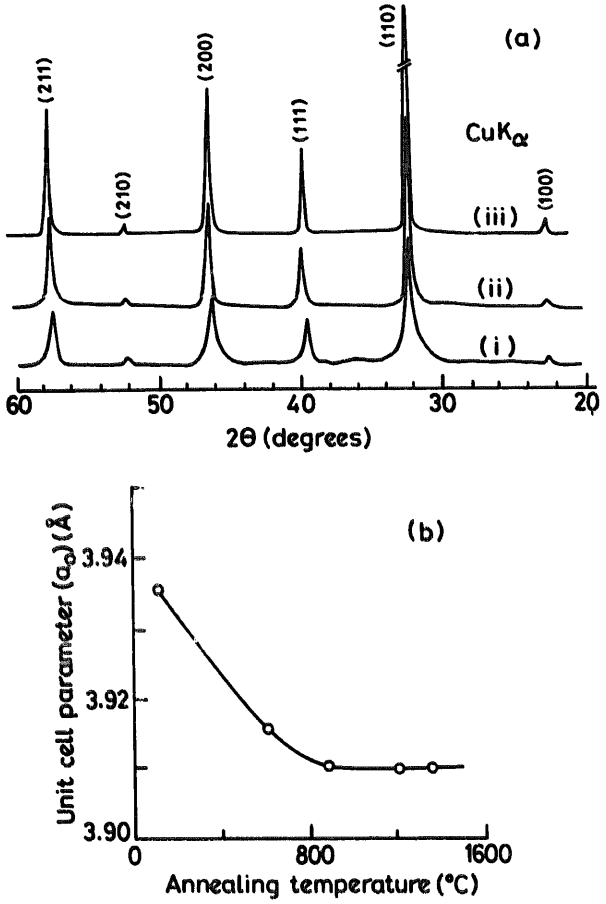

Fig. 1. (a) XRD patterns of $SrTiO_3$ samples: (i) as-prepared; (ii) annealed at 650 °C; (iii) annealed at 1100 °C. (b) Variation of unit cell parameter (a_0) vs. annealing temperature.

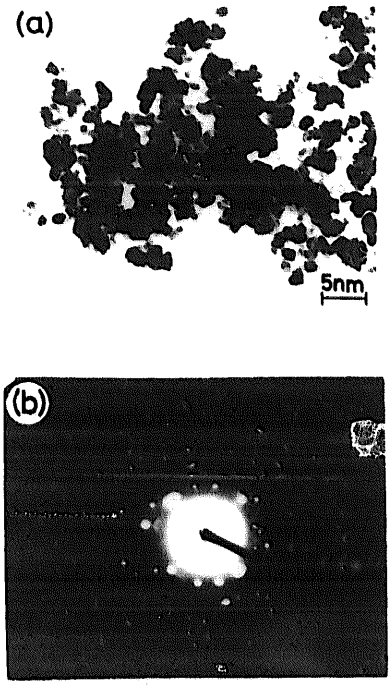

Fig. 2. Transmission electron micrograph of $SrTiO_3$ powder: (a) morphology of the as-prepared powder; (b) corresponding electron diffraction pattern.

Table 1
Physical characteristics of $SrTiO_3$ powders prepared through G–C conversion

Sample code	Annealing temperature (°C)	Surface area ($m^2 g^{-1}$)	Unit cell parameter (a_0) (Å)
SA-1	110	47.6	3.936
SA-2	650	46.1	3.916
SA-3	900	40.2	3.911
SA-4	1100	26.1	3.910
SA-5	1300	21.5	3.910
SA-6	1450	18.6	3.910

of decomposition. This corresponds to the retention of hydroxyl groups, which is confirmed by the IR absorption spectrum of weak intensities at 3560 and 650 cm^{-1}. Since the as-prepared powder has a larger unit cell parameter which decreases on heat treatment, this indicates that hydroxyl groups are retained within the perovskite lattice. The aliovalent OH^- replacing O^{2-} must be compensated by an equivalent number of cation vacancies to maintain electroneutrality. Thus the presence of framework modifiers enhances the concentration of lattice defects.

Singie crystalline $SrTiO_3$ has a band gap near 3.2 eV, corresponding to an absorption edge at approximately 387 nm. The optical absorption spectra of $SrTiO_3$ particle suspensions do not show any abrupt variations around 387 nm (Fig. 3(a)). This is in contrast with the spectra of $SrTiO_3$ single crystals and polycrystals with a grain size above 50 μm (Fig. 3(b)). The optical absorption continues to increase at lower wavelengths and shows an absorption maximum at 299 nm. The absorption maximum shifts to 261 nm with decreasing particle concentration. The optical absorption spectra of the particle suspensions can be discussed in comparison with the reported absorption spectrum of $SrTiO_3$ single crystal [24], where the A_1 peak is attributed to the $\tau_{15} \rightarrow \tau_{12}$ transition and A_2 to the $\tau_{25} \rightarrow \tau_{12}$ transition (Fig. 3(b)). The absorption maximum observed in Fig. 3(a) is attributed to the merging of these interband transitions. In the case of ultrafine particles, the band edge absorption is strongly affected even in the 5–20 nm size range.

3.2. Photodegradation studies

The kinetic data of the photodegradation of phenol are shown in Fig. 4. In the absence of other reactants, aqueous phenol does not degrade on UV irradiation. When mixed with $SrTiO_3$ particles and exposed to UV irradiation ($\lambda_{max} \sim 365$ nm), C/C_0 decreases to around 0.85 and then remains unchanged. The same results are obtained when phenol containing 250 mM H_2O_2 or $NaClO_3$ is irradiated in the absence of $SrTiO_3$. Photomineralization is observed only in the presence of $SrTiO_3$ and either H_2O_2 or $NaClO_3$. The results show

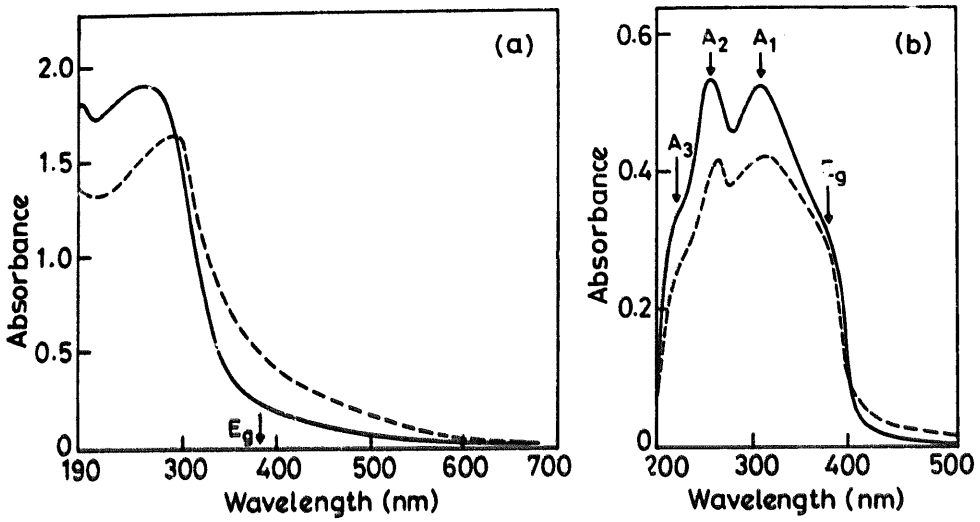

Fig. 3. Optical absorption spectra of $SrTiO_3$ particles at 25 °C: (a) suspensions in water (0.097 mg ml^{-1} (full line); 0.298 mg ml^{-1} (broken line)); (b) single crystal (full line) and polycrystalline ceramic sample of 50 μm grain size (broken line).

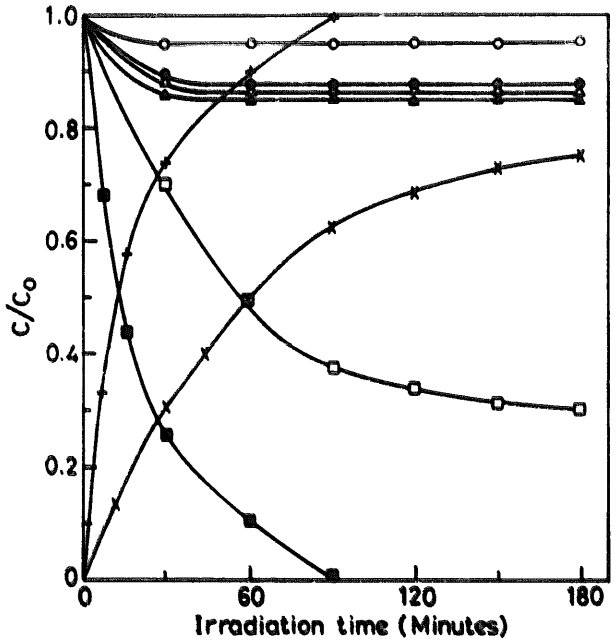

Fig. 4. Kinetics of phenol degradation (all curves on UV irradiation; $C_0 = 2$ mM; pH ~ 6.5): ○, phenol; ●, phenol and H_2O_2; △, phenol and $NaClO_3$; ▲, phenol and $SrTiO_3$; □, phenol, $SrTiO_3$ (SA-5) and 250 mM $NaClO_3$; ■, phenol, $SrTiO_3$ (SA-5) and 250 mM H_2O_2; ×, CO_2 evolution corresponding to □; +, CO_2 evolution corresponding to ■.

that H_2O_2 is more effective than $NaClO_3$ (Fig. 4). The rate of phenol degradation increases remarkably and more than 99% of the phenol disappears within 90 min when H_2O_2 is used. In comparison, 60% of the phenol disappears after 90 min when $NaClO_3$ is used.

$SrTiO_3$ samples were heat treated at temperatures in the range 110–1500 °C in order to investigate the effect of powder agglomeration and particle crystallinity on the photoreactivity. Fig. 5 illustrates the effect of heat treatment on the photocatalytic activity of $SrTiO_3$ powder. The results show that there is an increased reactivity with increasing annealing temperature; the maximum photocatalytic activity is observed for samples heat treated at 1100–1300 °C (SA-4 and SA-5), i.e. complete mineralization of phenol is achieved within 90 min for SA-5. For powders heat treated at 900 °C (SA-3), complete phenol destruction occurs after 180 min. The high activity for SA-5 may be attributed to the fact that, as the annealing temperature is increased, the nature of the charge trap centres is altered, as shown by the EPR data presented in the next section. This is in spite of the fact that the surface area of the catalyst decreases from 47.6 to 21.5 $m^2\ g^{-1}$ on annealing. Heat treatment at temperatures of 1350 °C or above

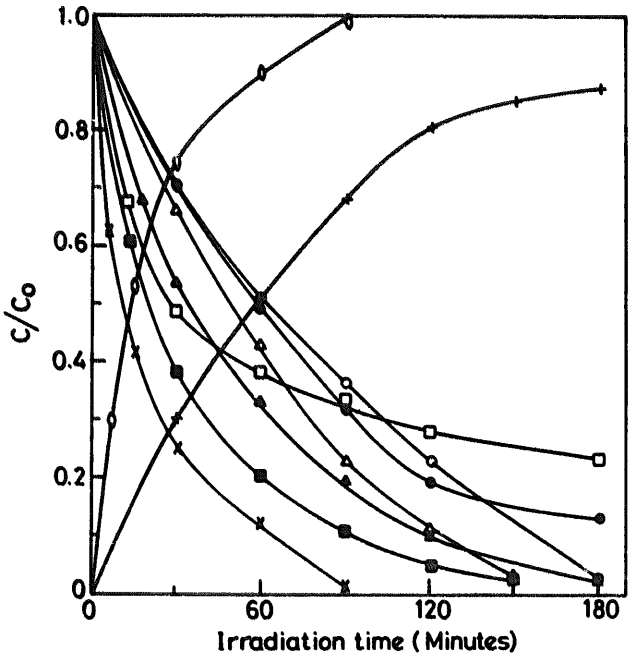

Fig. 5. Kinetics of phenol degradation: effect of annealing temperature ($C_0 = 2$ mM; pH ~ 6.5; $[H_2O_2] = 25$ mM): ●, SA-1; △, SA-2; ○, SA-3; ▲, SA-4; ×, SA-5; ■, SA-6; □, Degussa P25; 0, CO_2 evolution corresponding to ×; +, CO_2 evolution corresponding to ■.

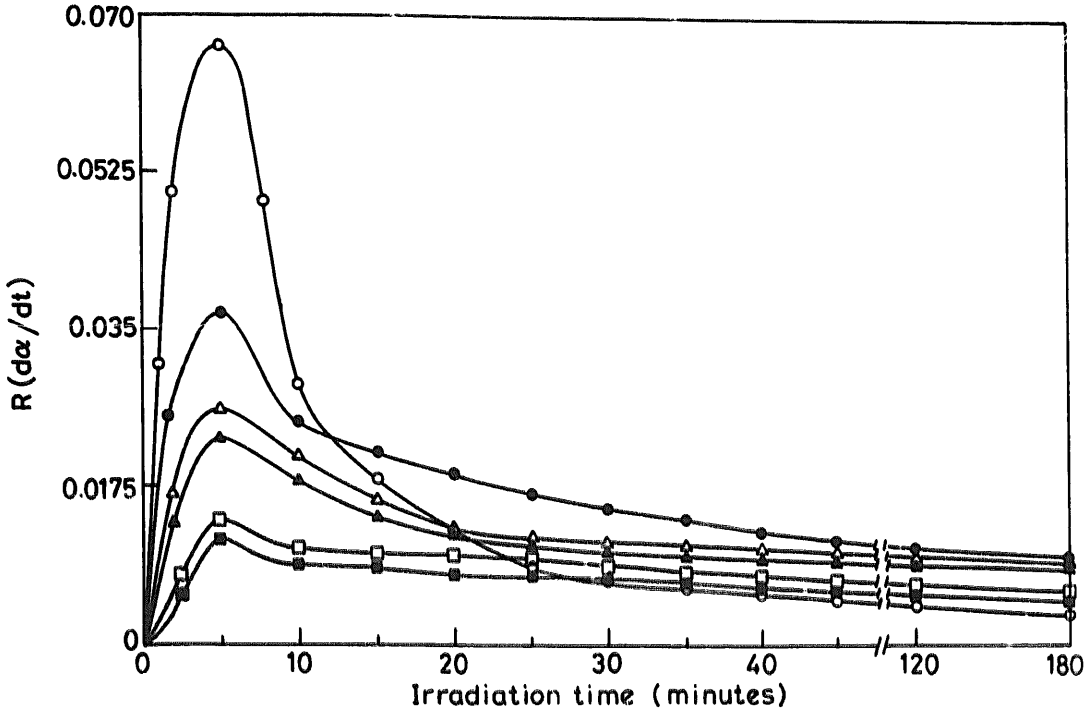

Fig. 6. Rate curve for phenol degradation: effect of annealing temperature (C_0 = 2 mM; pH ~ 6.5; [H_2O_2] = 25 mM): ○, SA-5; ●, SA-6; △, Degussa P25; ▲, SA-4; □, SA-2; ■, SA-3.

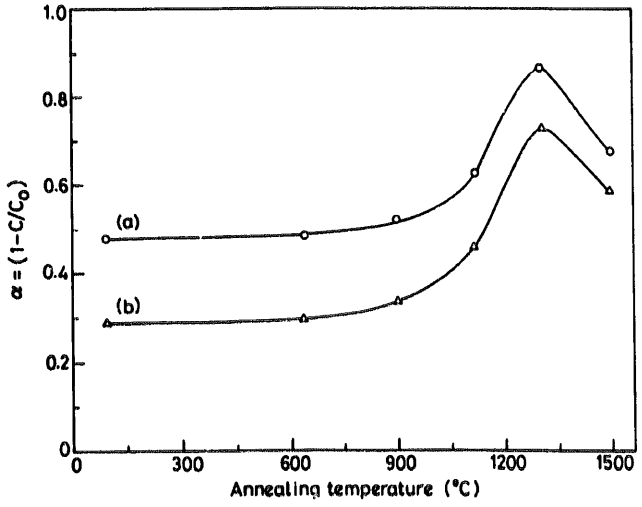

Fig. 7. α vs. annealing temperature (C_0 = 2 mM; pH ~ 6.5; [H_2O_2] = 25 mM): (a) α at 60 min; (b) α at 30 min.

leads to a decrease in the photoactivity of the catalyst, because of grain growth through sintering and recrystallization processes. In comparison, a sample of commercially available TiO_2 (Degussa P25, as-received powder from the manufacturer) is less active (Fig. 5). It is evident from Fig. 6 that SA-5 shows the maximum rate with an R value ($= d\alpha/dt$, where α is the fraction of the pollutant degraded, i.e. $\alpha = 1 - C/C_0$, and t is the time) of 0.06 compared with 0.022 for Degussa P25 and 0.04 for SA-6. A plot of α vs. the annealing temperature (Fig. 7) shows only a marginal increase in reactivity up to 900 °C, followed by a considerable increase up to 1300 °C. The rate decreases when the powders are annealed at 1350 °C or above.

The photocatalytic activity of the 900 °C annealed sample (SA-3) is enhanced when the H_2O_2 concentration is increased from 25 to 250 mM (Fig. 8). Under these condi-

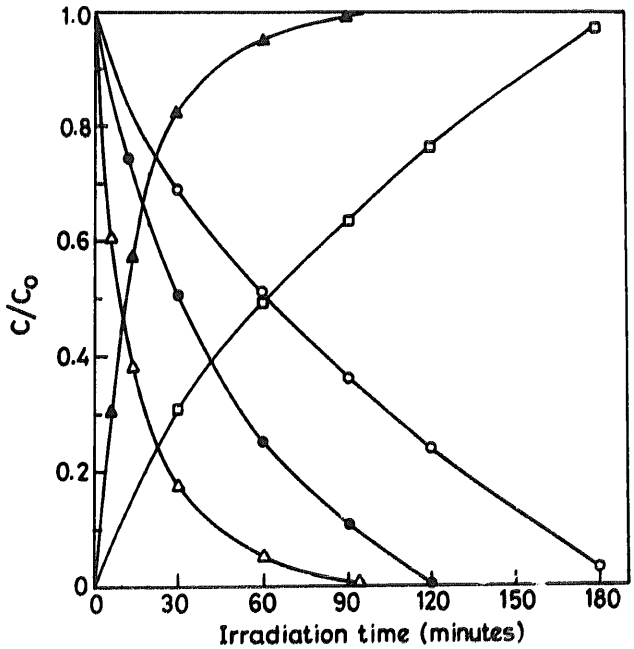

Fig. 8. Kinetics of phenol degradation: effect of H_2O_2 concentration (C_0 = 2 mM; catalyst is SA-3; pH ~ 6.5): ○, 25 mM H_2O_2; ▲, 82.5 mM H_2O_2; △, 250 mM H_2O_2; ▲, CO_2 evolution corresponding to △; □, CO_2 evolution corresponding to ○.

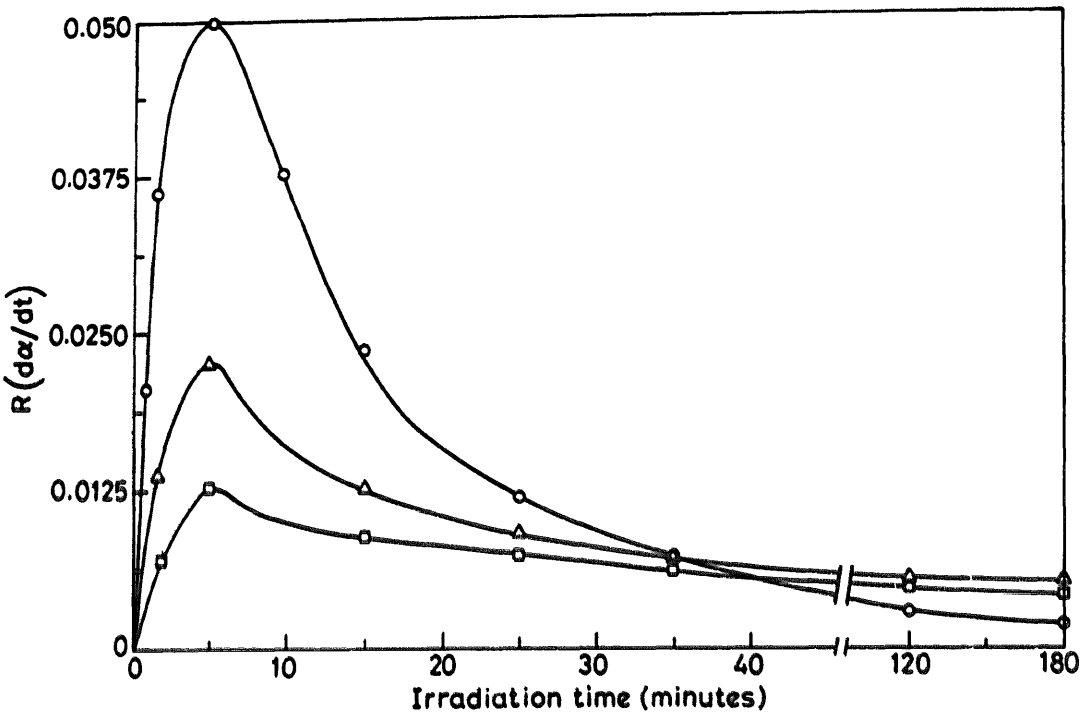

Fig. 9. Rate curve for phenol degradation: effect of H_2O_2 concentration ($C_0 = 2$ mM; catalyst is SA-3; pH ~ 6.5): ○, 250 mM H_2O_2; △, 82.5 mM H_2O_2; □, 25 mM H_2O_2.

tions, phenol is completely photomineralized within 100 min. The corresponding rate curve (Fig. 9) shows an R_{max} value of 0.05 when the ratio of $[H_2O_2]/[\text{phenol}]$ is 125 compared with an R_{max} value of 0.013 when the ratio of $[H_2O_2]/[\text{phenol}]$ is 12.5.

The kinetic data show that $SrTiO_3$ particles alone are inefficient in the photocatalytic degradation of phenol. Photocatalytic activity is exhibited only in the presence of oxidizing agents, such as H_2O_2 or $NaClO_3$, on illumination. Furthermore, phenol does not degrade in the presence of the oxidizing agent on illumination without $SrTiO_3$. Therefore a homogeneous photolytic degradation can be ruled out. Fig. 10 shows that the extent of the reaction increases with an increase in H_2O_2 to a certain level, and then α levels off without an apparent decrease in the photodegradation rate with a further increase in H_2O_2 concentration. This result cannot be explained on the basis of the formation of OH• from H_2O_2, the former being adsorbed onto the surface of the particle. If OH• produced from H_2O_2 were the reactive intermediate, the mineralization of phenol should proceed to completion under homogeneous conditions. Other oxidizing agents, such as $NaClO_3$, which do not generate OH•, are also effective, indicating that the photomineralization is independent of hydroxyl radicals as intermediate. However, the results are indicative of the electron scavenging capability of H_2O_2, thereby preventing the recombination between photogenerated electrons and holes. In general, the involvement of OH• as a charge transfer intermediate is not substantiated by the present results.

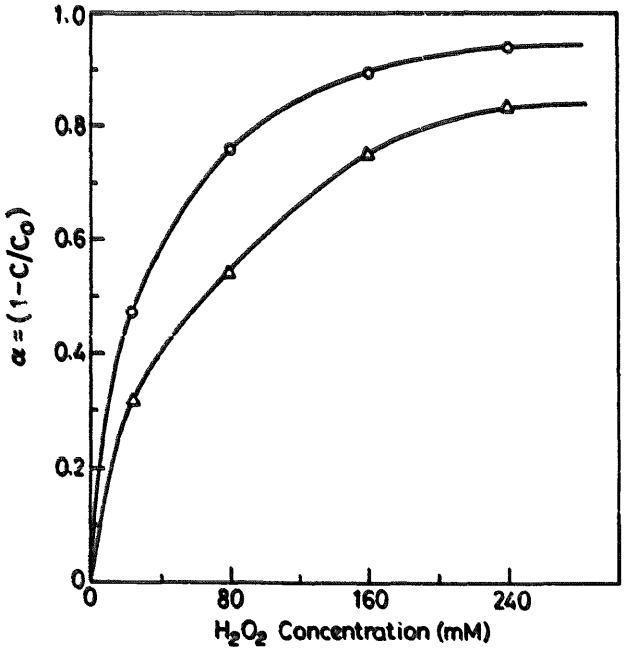

Fig. 10. α vs. H_2O_2 concentration ($C_0 = 2$ mM; catalyst is SA-3; pH ~ 6.5): ○, α at 60 min; △, α at 30 min.

3.3. EPR studies of the charge trap centres

The charge transfer process in $SrTiO_3$ during the photodegradation of pollutants is greatly affected by the nature of the trap states prevailing in the solid. Electrons and holes are formed when the semiconductor particles are irradiated with UV light. These charge carriers can be partly trapped at the

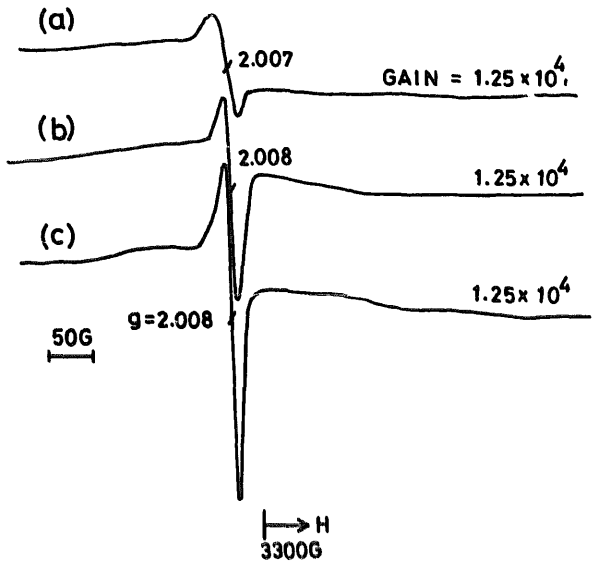

Fig. 11. EPR spectra of $SrTiO_3$ powders recorded between 78 and 300 K: (a) as-prepared catalyst, unirradiated; (b) as-prepared catalyst recovered after irradiation; (c) as-prepared catalyst recovered after irradiation (recorded at 78 K).

point defects before they are transferred across the interface. Figs. 11–13 show the EPR spectra of $SrTiO_3$ powders recovered from the photodegradation experiments.

The as-prepared powders of $SrTiO_3$ from the G–C conversion route show an EPR signal of $g=2.007$; this signal is asymmetric, but lacks any fine structure (Fig. 11). Considering the fact that $\Delta g = g_{obs} - g_e$ (where $g_e = 2.0023$ is the free electron value) is positive, the signal can be assigned to a hole centre. On annealing in an atmosphere of $N_2 + H_2$ at 900 °C, this signal disappears, which is characteristic of a hole centre. When $Ti/Sr > 1$ in the preparation medium, the signal intensity increases, implying that the trapped hole has a higher stability in titanium-rich but strontium-deficient compositions. When the prepared powder is dispersed in dilute HNO_3 (0.05 M) and further washed in distilled water, the hole centre signal increases in intensity. Sr^{2+} ions are detected in the filtrate by atomic absorption spectroscopy (AAS) but no Ti^{4+}. This experiment demonstrates that the stability of the hole centre can be correlated with the strontium vacancy (V_{Sr}) concentration at the surface region. The notations of Kröger [25] for the defect sites, widely used in solid state chemistry, are employed in this paper. Similar treatment of $SrTiO_3$ powder in dilute acetic acid leads to a decrease in the intensity of the signal, because of the hole scavenging capability of the acetate ion. These experiments indicate that hole centres are located in the surface region rather than in the bulk of the particles. Furthermore, on heating the acid-treated sample above 900 °C, the intensity decreases. This is accompanied by a decrease in surface area, indicating that the hole centres are located mainly in the surface region [26]. The signal does not arise from hydroxyl radicals for the following reasons. Riederer et al. [27] have reported that $OH^{\bullet}$ in a semicrystalline matrix can have $g_x = g_y = 2.008$ and g_z

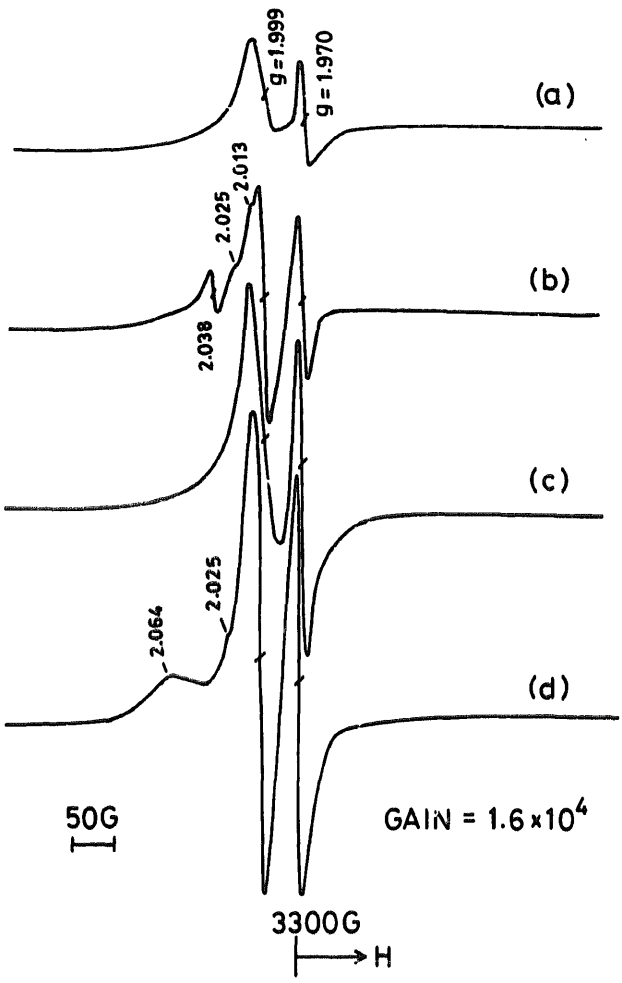

Fig. 12. EPR spectra of $SrTiO_3$ powders recorded at 78 K: (a) SA-2, unirradiated; (b) SA-2, recovered after irradiation; (c) SA-3, unirradiated; (d) SA-3, recovered after irradiation.

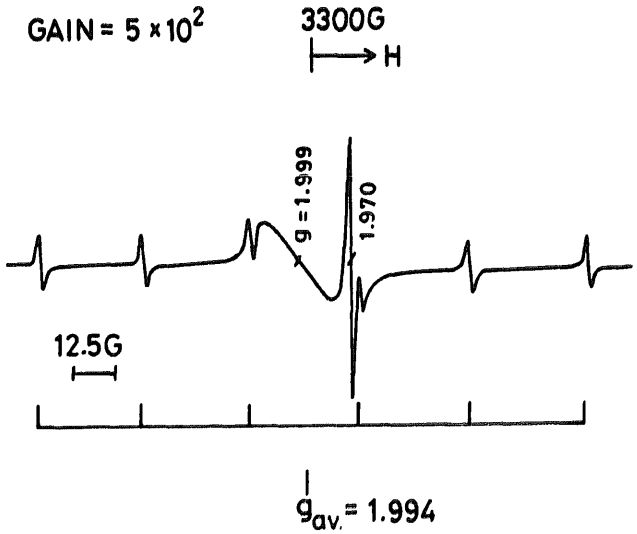

Fig. 13. EPR spectrum of $SrTiO_3$ powders recorded at 78 K, catalyst SA-4, unirradiated. (The catalyst recovered after irradiation gave a similar EPR spectrum.)

varying from 2.05 to 2.25. Since the fine structure is absent, particularly the high g value component for the present signal, it cannot be assigned to OH', whereas the signal can be more favourably assigned to $(Ti^{4+}–O^-)_s$ centres. Hydroxyl radicals have been reported to be undetectable on TiO_2 by EPR methods; radical trapping by organic compounds is said to be necessary for their detection [28]. However, hydroxyl radicals have been detected by EPR in many solids mentioned in the references cited in Ref. [27] and also in minerals [29], where the multiplicity of the EPR fine structure has been noted.

The signal of $g = 2.007$ disappears when the annealing temperature of the powders in air is greater than 900 °C. For these powders, additional signals are observed with $g = 1.970$ arising from the $Ti^{3+}–V_O$ defect complex and $g = 1.999$ (Fig. 12) arising from the singly ionized strontium vacancy V'_{Sr} reported previously [26]. These signals do not arise from Fe^{3+} impurity, which has a similar g value, since the signals are not observed for the powders annealed at lower temperatures. Furthermore, the intensities of these signals increase on annealing in an $N_2 + H_2$ atmosphere, and also at higher heat treatment temperatures. Aqueous suspensions of $SrTiO_3$ powders annealed in air at 900 °C on irradiation give rise to additional signals with g values of 2.013, 2.026 and 2.038. These signals arise from the same centres with orthorhombic symmetry, since their relative intensities show a parallel variation with changing microwave power, chemical treatment and temperature. These signals have previously been assigned to $V_{Sr}–O^-–Ti^{4+}$ defect centres, where the hole trapped at the strontium vacancy is delocalized on the neighbouring anion. As the temperature of annealing is increased to above 1000 °C, the signals decrease in intensity after irradiation; they are totally absent for powders heat treated above 1100 °C, even after long-term irradiation. Therefore the hole centres are unstable in powders annealed above 1000 °C after irradiation. When manganese impurity is present as a dopant in $SrTiO_3$, the EPR spectrum shows the six-line signal (Fig. 13) arising from the hyperfine components of the ^{55}Mn nuclei. The average g value of these signals is 1.994, which corresponds to that of Mn^{4+} reported in $SrTiO_3$ by Müller and coworkers [30,31]. The intensity of the Mn signals does not change after irradiation, implying that Mn_{Ti} does not participate in the charge transfer process, being located in the grain interior. Fig. 14 shows the variation in intensity arising from the electron centres, namely $Ti^{3+}–V_O$ (or, more descriptively, $Ti^{3+}–V_O–Ti^{4+}$, i.e. an electron captured at the oxygen vacancy in the titanate perovskite structure which is delocalized between the two adjacent Ti^{4+} ions) and V'_{Sr} after annealing at various temperatures. Although the $g = 1.970$ intensity steadily increases with increasing annealing temperature, $g = 1.999$ arising from V'_{Sr} goes through a maximum. This difference in the effect of the annealing temperature can be attributed to the subsurface contribution of V'_{Sr} compared with the bulk location of the $Ti^{3+}–V_O$ complex. Surface passivation followed by secondary particle agglomeration, leading to partial sintering, accounts for the

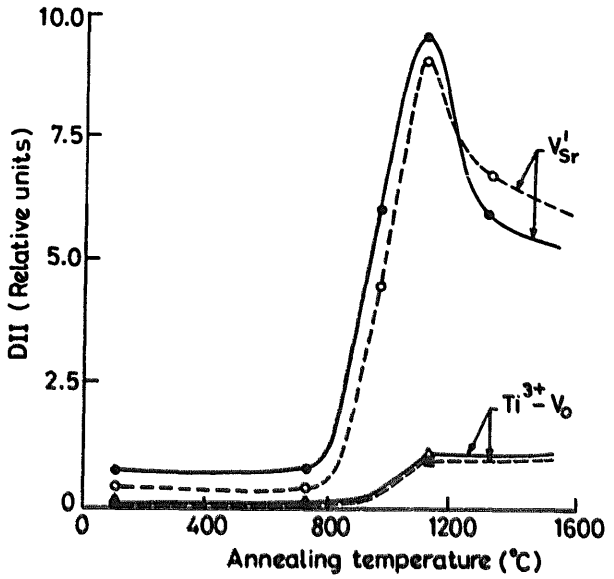

Fig. 14. Double integrated intensity (DII) of the EPR signals vs. the sample annealing temperature.

decreased intensity of the V'_{Sr} signal after annealing at high temperatures.

The effect of annealing the powders at high temperatures on the photocatalytic activity of $SrTiO_3$ can be explained in the following way. In the as-prepared powder, $(Ti^{4+}–O^-)_s$ hole centres localized at the surface region participate in the hole transfer process from the solids to the organic substrate. In addition, the mediation of $Ti^{4+}–O^-–V_{Sr}$ in the hole transport process can be expected for powders annealed at less than 900 °C. In general, these centres slow down the transfer of photogenerated holes via decreasing diffusion length as well as the diminished mobility of positive charge carriers. These centres are unstable on annealing above 900 °C, whereas electron centres, such as $Ti^{3+}–V_O$ and V'_{Sr}, are stabilized at higher temperatures. The EPR results show that the intensity of V'_{Sr} goes through a maximum as the annealing temperature is increased. In comparison, the intensity of $Ti^{3+}–V_O$ increases continuously with the annealing temperature. It has been reported in the literature that donor states, such as $Ti^{3+}–V_O$, will be located nearer to the conduction band edge. The energy levels of the acceptor centres, such as V'_{Sr}, will be closer to the valence band [12,32]. In fact, the cation vacancies disrupt the chemical bonds with O^{2-}, thereby perturbing the filled valence bands of titanates made up of $2p^6$ orbitals of O^{2-} and creating acceptor states. If these acceptor states are not lifted out of the valence band, they will remain neutral. In the as-prepared $SrTiO_3$ powders, lifting of the V_{Sr}-related acceptor states is incomplete. As the powder is annealed at temperatures above 900 °C, discrete levels are generated above the valence bands which can capture electrons to form localized states within the band gap to become V'_{Sr}. Since the conversion of neutral cation vacancies to singly ionized vacancies is incomplete, they overlap with the valence band; therefore the photogenerated holes travel uphill, finding their way through neutral strontium vacancies

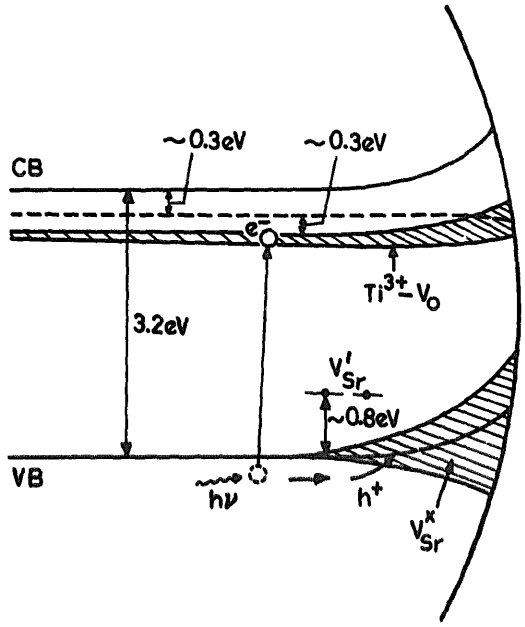

Fig. 15. Schematic diagram of the energy levels for the native point defects in cubic $SrTiO_3$ (after Refs. [12] and [32]).

(Fig. 15). These holes are available at the interface for reaction with the organic molecules, irrespective of the value of their redox potentials relative to the valence band edge. As the annealing temperature is increased above 1100 °C, most of the neutral vacancies convert to the ionized form, thereby decreasing the rate of hole transfer. In an analogous way, the electron transfer from $Ti^{3+}-V_O$ centres to H_2O_2 or other oxidizing species can also be envisaged. In both ways, the separation of photogenerated holes from electrons is facilitated by the mid-band gap states within the semiconductor particle. The concentration of the cation vacancies in the titanate semiconductor is directly related to the preparation route, the significance of which has been presented earlier.

4. Conclusions

The present results show that $SrTiO_3$ and alkaline earth titanates, in general, can be used as photocatalysts for the degradation of organic pollutants. The photoactivity is related to the preparative route of the powders. In comparison with all the well-known low temperature chemical routes for the preparation of $SrTiO_3$ powders, the gel to crystallite conversion reported here can yield nanometre-sized particles with a high surface area. The present results show that defect centres participate in the charge transfer process during photocatalytic reactions, as shown by the EPR results of the $SrTiO_3$ powders recovered from degradation experiments.

References

[1] R.W. Matthews, *J. Catal.*, *97* (1986) 565.
[2] A.L. Pruden and D.F. Ollis, *J. Catal.*, *82* (1983) 404.
[3] A. Sclafani, L. Palmisano and E. Davi, *New. J. Chem.*, *14* (1990) 265.
[4] A. Mills and P. Sawunyama, *J. Photochem. Photobiol. A: Chem.*, *84* (1994) 305.
[5] M. Schiavello, *Electrochim. Acta*, *38* (1993) 11.
[6] W. Lee, Y.-M. Gao, K. Dwight and A. Wold, *Mater. Res. Bull.*, *27* (1992) 685.
[7] A.J. Hoffman, E.R. Carraway and M.R. Hoffmann, *Environ. Sci. Technol.*, *28* (1994) 776.
[8] G. Dagan, S. Sampath and O. Lev, *Chem. Mater.*, *7* (1995) 446.
[9] C. Anderson and A.J. Bard, *J. Phys. Chem.*, *99* (1995) 9882.
[10] A. Kudo, A. Tanaka, K. Domen and T. Onishi, *J. Catal.*, *111* (1988) 296.
[11] Q.S. Li, K. Domen, S. Naito, T. Onishi and K. Tamaru, *Chem. Lett.*, *3* (1983) 321.
[12] T.R.N. Kutty and M. Avudaithai, in L.J. Tejuca and J.L.G. Fierro (eds.), *Properties and Applications of Perovskite Type Oxides*, Marcel Dekker, New York, 1993, p. 307.
[13] N. Christen and S.E. Ramussen, *Acta Chem. Scand.*, *17* (1963) 845.
[14] M. Avudaithai and T.R.N. Kutty, *Mater. Res. Bull.*, *22* (1987) 641.
[15] P.K. Gallagher and F. Schrey, *J. Am. Ceram. Soc.*, *46* (1963) 567.
[16] H.S.G. Murthy, M. Subbarao and T.R.N. Kutty, *Thermochim. Acta*, *13* (1975) 183.
[17] M.I.D. Guemes, T.G. Carreno, C.J. Serna and J.M. Palacios, *J. Mater. Sci.*, *24* (1989) 1011.
[18] K.R. Thampi, M. Subbharao, W. Schwarz, M. Grätzel and J. Kiwi, *J. Chem. Soc., Faraday Trans. 1*, *5* (1988) 1703.
[19] T.R.N. Kutty and P. Padmini, *Mater. Res. Bull.*, *27* (1992) 945.
[20] P. Padmini and T.R.N. Kutty, *J. Mater. Chem.*, *4* (1994) 1875.
[21] T.R.N. Kutty and P. Padmini, *Mater. Chem. Phys.*, *39* (1995) 200.
[22] T.R.N. Kutty and S. Ahuja, *Mater. Res. Bull.*, *30* (1995) 233.
[23] H.J. Taras, A.E. Greenberg, R.D. Hoak and M.C. Rand (eds.), *APHA-AWWA-WPCF, Standard Methods for the Examination of Water and Waste Water*, American Public Health Association, Washington, DC, 13th edn., 1971.
[24] M. Cardona, *Phys. Rev.*, *140* (1965) A651.
[25] K.A. Kröger, *The Chemistry of Imperfect Crystals*, Vols. 1–4, North-Holland, Amsterdam, 1974.
[26] T.R.N. Kutty and M. Avudaithai, *Mater. Res. Bull.*, *25* (1990) 821.
[27] H. Riederer, J. Huttermann, P. Boon and M.C.R. Symons, *J. Mag. Res.*, *54* (1983) 54.
[28] R.F. Howe and M. Grätzel, *J. Phys. Chem.*, *89* (1985) 4494.
[29] M.J. Samailovich and A.I. Novozhilov, *Zh. Neorg. Chim.*, *15* (1970) 84.
[30] K.A. Müller, *J. Phys.*, *42* (1981) 551.
[31] K.W. Blazey, J.W. Cabreraad and K.A. Müller, *Solid State Commun.*, *45* (1983) 903.
[32] T.R.N. Kutty and L. Gomathidevi, *Mater. Res. Bull.*, *20* (1985) 793.